

Predicting Treatment Options for the  
Intervertebral Disc:  
Patient-Specific  
Finite Element Models

by  
Sonia R. Ahrens

A THESIS

submitted to

Oregon State University  
Honors College

in partial fulfillment of  
the requirements for the  
degree of

Honors Bachelors of Science  
in Bioengineering  
(Honors Scholar)

Presented April 2, 2019  
Commencement June 2019



## ABSTRACT

Sonia R. Ahrens for the degree of Honors Bachelor of Science in Bioengineering presented on April 2, 2019.

Title: Predicting Treatment Options for the Intervertebral Disc: Patient-Specific Finite Element Models

Abstract Approved: \_\_\_\_\_

Morgan B. Giers

*This work describes a method for incorporating patient data into a nutrient transport model of the intervertebral disc. This data was collected using MRI diffusion weighted imaging (DWI), and was converted into an apparent diffusion coefficient map (ADC map). This map was used to define the diffusion behavior of water within the nucleus pulposus (NP), a value which was then scaled to yield the diffusivities of the three primary solutes selected for this model: glucose, oxygen, and lactate. The results show distinct diffusion behavior between patients, even within discs of the same Pfirrmann grade. The importance of the distinct disc morphologies and physiological environments of each patient to the diffusion gradients in the disc is readily apparent. Patient-specific models could allow clinicians look for critical concentrations and pH's in the patient's discs (i.e. levels below which cells cannot survive). If levels are already low enough to indicate cell death, these patients would not be candidates for cell injection-based therapies. For patients without a dead zone - who are therefore candidates for cell therapy - the model can be used to determine proper dosing via iteratively increasing cell concentration until the patient develops a dead zone. This functionality indicates that patient-specific models could prove valuable in a clinical setting when predicting patient outcomes or treatment options.*

*See Appendix A for a summary of abbreviations and key terms*

KEY WORDS: Intervertebral Disc (IVD), back pain, transport modeling, diffusion weighted imaging (DWI)

Corresponding Email Address: ahrenss@oregonstate.edu

© Copyright by Sonia R. Ahrens  
April 2, 2019

Predicting Treatment Options for the  
Intervertebral Disc:  
Patient-Specific  
Finite Element Models

by  
Sonia R. Ahrens

A THESIS

submitted to

Oregon State University  
Honors College

in partial fulfillment of  
the requirements for the  
degree of

Honors Bachelors of Science  
in Bioengineering  
Honors Scholar

Presented April 2, 2019  
Commencement June 2019

Honors Baccalaureate of Science in Bioengineering project of Sonia R. Ahrens presented on April 2, 2019.

APPROVED:

---

Morgan Giers, Mentor, representing Bioengineering

---

Adam Higgins, Committee Member, representing Bioengineering

---

Aaron Fields, Committee Member, representing Orthopedic Surgery at UCSF

---

Toni Doolen, Dean, Oregon State University Honors College

I understand that my thesis will become part of the permanent collection of Oregon State University libraries. My signature below authorizes release of my thesis to any reader upon request.

---

Sonia R. Ahrens, Author

## ACKNOWLEDGEMENTS

The author expresses sincere appreciation to the following parties:

Dr. Morgan Giers for acting as the primary thesis research mentor and providing valuable guidance for every aspect of this project.

Ward Shalash for his assistance in developing patient-specific models.

Dr. Vadim Byvaltsev of Irkutsk State Medical University for his procurement of the patient data used in this investigation.

Dr. Aaron Fields for his insight into nutrient transport and compression modeling, which greatly influenced this work.

Oregon State University and the department of Chemical, Biological and Environmental Engineering for providing the funding and facilities for this research.

&

The Honors College for encouraging and facilitating this research project, providing resources, advising and funding this project with the DeLoach Work Scholarship.

## Contents

INTRODUCTION.....	1
Back Pain and IVD Degeneration	
Structure and Function of IVD	
IVD Transport Modeling: A Clinical Approach	
MATERIALS AND METHODS.....	6
Patient Data Collection: MRI Methodology	
Data Processing: MATLAB Methodology	
Patient Models: COMSOL Methodology	
RESULTS AND DISCUSSION.....	15
Model Analysis	
Model Limitations & Future Work	
CONCLUSION.....	18
Appendix 1 – Index of Abbreviations	
Appendix 2 – Supplemental Figures	
Appendix 3 – COMSOL Constants and Equations	



## INTRODUCTION

### Back Pain and IVD Degeneration

Back pain is the leading cause of disability worldwide.<sup>1</sup> Experts estimate that up to 80% of the population will eventually experience some form of back pain.<sup>2</sup> This affliction is costly, both to individuals and society at large. Quality of life becomes the main concern for individuals who may suddenly find themselves unable to perform basic tasks, including participating in the workforce. Back pain places patients under a twofold economic strain; not only do they accrue debt from medical expenses, but they may also suffer lost wages or, in some cases, jobs. A recent study determined the total annual costs associated with lower back pain (LBP) in the United States exceeded \$100 billion.<sup>3</sup> Two-thirds of these costs were a result of lost wages and lost productivity.

Though the impact of LBP has been thoroughly characterized, its origin is not totally understood. However, research indicates that a primary source of LBP may be degeneration of the cartilage discs in the spine.<sup>4-7</sup> Disc degeneration is a phenomenon that has become increasingly associated with LBP, particularly the later stages of degeneration – as characterized by Pfirrmann grades<sup>4 & 58,9</sup> – which may even include disc herniation (a summary of Pfirrmann grade classifications can be found in Appendix 2, Figure 2e). The injury and repair of the degenerated areas of the disc can lead to neo-innervation and neovascularization of the annulus fibrosus and nucleus pulposus, which could also contribute to pain.<sup>10</sup> Degeneration of the intervertebral disc (IVD) can be caused by trauma or disease, but is most frequently a product of aging. Aging causes chemical and structural changes in and around the disc, which can disrupt the disc's delicate metabolite equilibrium.<sup>10</sup> This equilibrium is so precarious simply due to disc's unique structure and nutrient supply.

### Structure and Function of IVD

The IVD is the largest avascular structure in the human body, and thusly IVD cells are dependent on the mechanism of diffusion to receive nutrients.<sup>11</sup> The IVD's primary substructures include the annulus fibrosus (AF), nucleus pulposus (NP) and cartilaginous endplate (CEP). External structures include the vertebral bodies (made up of cancellous bone surrounded by a shell of cortical bone) which interface with the discs through the bony endplate (BEP).<sup>10</sup> Disc homeostasis relies primarily on the mechanism of

diffusion through the CEP, both to deliver nutrients (glucose and oxygen, among others) to cells in the NP, and AF and to remove unwanted metabolites (lactic acid, among others) from disc tissue. A sectioned diagram of these structures and associated nutrient diffusion pathways by Urban et al can be found in Appendix B, along with a labeled image of a dissected lumbar porcine IVD.

IVD cells must cope with a harsh environment: they suffer from near-consistent nutrient deprivation, endplate calcification, buildup of metabolic byproducts, extreme pH, and consistent mechanical strain. Disc cells – particularly those in the center of the NP – contend with large nutrient diffusion distances and slow diffusion speeds. This can prevent adequate nutrients from reaching these cells, which are already relatively sparse, leading to suppressed cell activity and tissue maintenance, and eventually cell death.<sup>4,12,13</sup> This state of nutrient deprivation is only exacerbated by cases of impaired blood supply. Impaired blood supply is a symptom of numerous diseases, which can act at the level of the disc, and its various substructures. These diseases include atherosclerosis of arteries in the lumbar spine and buildup of atherosclerotic plaques (common symptoms of smoking and diabetes<sup>14,15</sup>), sickle cell anemia, and structural changes including occlusion of the marrow spaces, calcification of the endplate, endplate sclerosis, Modic changes, Schmorl's nodes or endplate lesions.<sup>4</sup> Furthermore, a buildup of lactic acid in the disc due to diffusion limitations can cause a sharp drop in pH, which only serves to further stress IVD cells.

The primary function of the discs – which make up 15–20 % of the length of the spinal column – is absorbing biomechanical forces, and allowing movement of the spinal column.<sup>10</sup> By design, these structures must endure regular mechanical loading, which includes extremes of both loading (ex. carrying items) and unloading (ex. hanging upside-down). This loading has been shown to have both a positive and negative influence on cell viability in the disc. It decreases disc height, which reduces the diffusion distance for nutrients traveling from the CEP to cells at the center of the disc, but it also decreases the fluid content in the disc, which reduces solute diffusivities and increases cell metabolism, leading to further buildup of metabolic byproducts like lactic acid.<sup>16</sup>

With a complicated system like this, for which achieving homeostasis is an extremely precarious state, true characterization requires modeling of the specific conditions experienced by a given disc. Generic models are useful for developing a general theory, but

will likely be grossly inaccurate when applied to a specific disc, thereby making them clinically irrelevant. The work here seeks to address this discrepancy and lend direct clinical relevancy to the vast amount of research that has been conducted to characterize the human intervertebral disc and spine as a whole.

### IVD Transport Modeling: A Clinical Approach

Several groups have tackled modeling the metabolism of the intervertebral disc: J.G. Urban<sup>17,18</sup>, Stephen J. Ferguson<sup>19</sup>, Andrea Malandrino<sup>20</sup>, and Alicia R. Jackson<sup>21</sup>, among others<sup>22-24</sup>. These groups have each characterized key properties related to IVD metabolism and transport, some of which will be included in the model developed here.

Bibby (2005) established that excised disc tissue (in culture medium exposed to air and at pH 7.4) behaves very differently from that found in vivo, where oxygen, glucose, and pH are all low.<sup>17</sup> Oxygen consumption and glycolysis dropped markedly under these condition, and equations were derived that satisfactorily predicted this behavior. However, the group did not account for the effects of mechanical stress/strain on cell consumption and on diffusivities due to a lack of data.

Malandrino (2011) addressed this topic, and found mechanical loading significantly influenced oxygen and lactate concentration when large and prolonged volume changes were applied.<sup>20</sup> Loading/unloading changed both the tissue diffusivity and diffusion distances, and excessive or prolonged loading triggers a drop in cell density and a decrease in NP swelling pressure due to loss of proteoglycans, both of which are detrimental to the disc. With respect to oxygen deprivation, this group noted that the location of “critical regions” (critically low oxygen levels) depended strongly on patient specific characteristics. This group did not consider local cell matrix synthesis and viability in their investigation, and therefore the behavior of glucose was ignored. A similar omission was also made by Zhu (2012).<sup>22</sup>

However, Ferguson (2004) found that fluid flow did not actually enhance the transport of low-weight solutes, and additionally fluid changes occurring over the entire diurnal loading cycle had minimal influence on the transport of large molecular-weight solutes.<sup>19</sup> Though, it should be noted fluid flow and solute transport were not coupled in this model. Another group’s findings also support this conclusion: a finite element model developed by Giers (2016) indicated no significant difference between a traction-treated disc and a regular

degenerated disc, and an *in-vitro* traction study (which was used to inform model fluid velocities) actually showed a significant decrease in nutrient flow through the traction-treated, relative to the normal disc.<sup>24</sup> The group acknowledges that the model behavior may indicate that certain biomechanical aspects of physiologic stretching were not captured in the simplified math model, and notes that further characterization is necessary *in vivo* to understand exact structural changes that occur during loading/unloading.

Other groups have further characterized the behavior of metabolites in the disc, and their interactions. Soukane (2007) coupled model equations for glucose, oxygen and lactate. This study found that nutrient concentrations could fall below levels required to maintain cellular activity or viability under the following conditions: (1) a loss of endplate permeability, (2) increased rates of oxygen and glucose consumption or lactic acid production, and (3) a fall in diffusivity due to long-term dehydration.<sup>18</sup> This model incorporated work from Jackson (2009) which established fixed charge densities (FCD) for IVD tissues using a two-point conductivity approach.<sup>21</sup> This work established that incorporating the FCD during modeling is important for proper characterization of transport and mechanical behaviors of the disc. Specifically, this investigation determined that the FCD of AF tissue is significantly lower than that in NP tissue, a property which was incorporated into boundary conditions of the Soukane model. However, it should be noted that Jackson's model for ion diffusivity does not account for relative water content of the tissue, nor attempt to develop a relationship between the two properties.

In summary, though these investigations are paramount in establishing the groundwork of this investigation, they possess a number of limitations. Ultimately, they fail to incorporate the extreme variability that exists between patients, and even discs of the same Pfirrmann grade. This variability is inherent to different bodies, and may include the thickness of the endplates, the quality/magnitude of blood supply, the specific disc sizing and tissue ratios, daily loading patterns and intensity (associated with the patient's career and hobbies) etc. With this previous work in mind, the present project takes advantage of these intrinsic characteristics of IVD structure and function, but also seeks to personalize these models to make them clinically relevant. Patient-specific models can account for a number of characteristics simultaneously that would otherwise need to be characterized separately and applied.

In this investigation, patient-specific models were developed via integration of patient data into key model parameters, namely diffusion behavior within the disc nucleus. Historically, this nucleus shows the most variability between discs, even at similar stages of degradation, and therefore should be able to showcase unique patient trends. This data was collected with MRI – specifically, diffusion weighted imaging (DWI) – which provided both diffusion maps and morphology of the disc tissue. Integrating this data into the model personalizes it to the patient and, pending further development, has the potential to be utilized in a diagnostic setting when selecting treatment methods.

Current treatments for disc degeneration and associated pain include the following: (1) conservative therapy, (2) discectomy, (3) disc replacement with prosthetic devices, and (4) spinal fusion surgery. Unfortunately, these treatments often show limited success.<sup>25</sup> Alternative treatments, which are currently under investigation, focus more on targeting molecular pathways of extra cellular matrix (ECM) degeneration. This is typically accomplished by injecting cells to supplement the limited number in tissue, increasing production of anabolic factors (by introducing growth factors), or by decreasing production of catabolic factors. These strategies overlook the challenge of increasing cell activity or density in a nutrient-starved environment, which must be included to properly anticipate treatment outcomes. The model developed here is intended to be used as a tool (pending further development) to help physicians further tailor these treatments to patients, thereby improving patient outcomes.

## MATERIALS AND METHODS

### Patient Data Collection: MRI Methodology

The full MRI methodology can be found in Belykh 2017.<sup>26</sup> Briefly: T1-weighted, T2-weighted and DWI images were taken of 100 consecutive patients admitted to the spinal surgery service at the Irkutsk Scientific Center of Surgery and Traumatology for vertebral fusion surgeries. This population excluded patients with spinal pathologies at levels other than lumbar, or those with tumors or vascular pathology. Imaging was performed on a 1.5 T Siemens Magnetom Essenza scanner (Siemens Healthineers, Erlangen, Germany), with sagittal slices of the lumbar spine collected for each patient. These slices were 4 mm thick with a consistent 30 x 30 cm field of view. DWIs were collected at 3 different b-values ( $b = 50, 400, 800 \text{ s/mm}^2$ ) using a body coil with a TR of 3000 ms, TE of 93 ms, 6 averages, and a matrix size of 156 x 192. This study was approved by the Institutional Ethics Committee at the Irkutsk Scientific Center of Surgery and Traumatology. Data was de-identified prior to its receipt by the Giers' Laboratory and therefore no Institutional Review Board approval is necessary from Oregon State University.

### Data Processing: MATLAB Methodology

DWI images were first converted into apparent diffusion coefficient (ADC) maps.

The patient data was extracted from the original MRI DICOM file to MATLAB (version 9.5) where it could be accessed for further processing. These data files were processed with a MATLAB program in which the slice level (1, 2, or 3) was selected, and the full lumbar image was cropped down to a single disc by the user (Figure 1). Any negative/infinite points were removed (replaced with a zero), and the ADC values were calculated with the following equation, which is simply a modification of the Stejskal-Tanner equation as established by Le Bihan<sup>27,28</sup>:

$$ADC = \ln \left( \frac{S_0}{S} \right) * \left( \frac{1}{b} \right) \quad (1)$$

Where  $S_0$  is the fitted value for signal intensity when  $b = 0$ ,  $S$  is the signal intensity provided by the DWI, and  $b$  is the gradient value. Diffusion characterization capability increases with the b-value. The maximum ADC value for the disc was noted for scaling purposes (Table 1) before the file was saved (.bmp) for use in COMSOL.

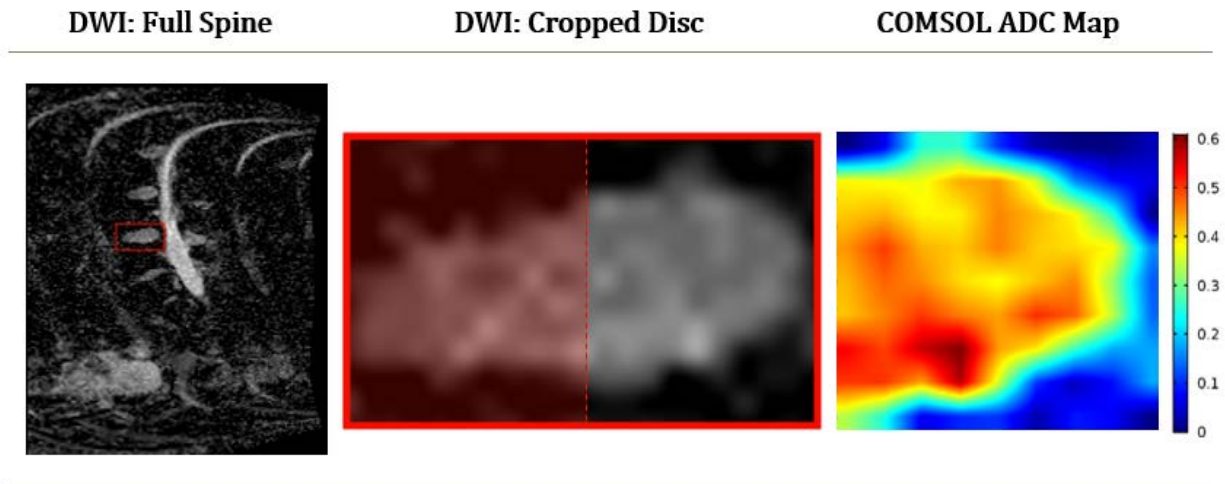


**Figure 1** – Image processing stages for Patient #1: the diffusion weighted image (DWI) of the whole spine with contrast enhancement (left), the cropped disc segment selected for modeling (middle), and the final clipped disc image as used in COMSOL. Note that the final image is clipped in half, allowing it to be wrapped 360° around the axis of symmetry assigned to the left y-axis, yielding the cylindrical shape that approximates that of a spinal disc (Figure 4).

**Table 1** – Maximum values identified for both the ADC image (determined in MATLAB) and normalized COMSOL image. A ratio of these values was used to convert each image back to the desired ADC scale after being imported into COMSOL as a normalized image. Disc selections are shown in Figure 2c of Appendix 2.

Patient	MATLAB (ADC) Max [m <sup>2</sup> /s]	COMSOL Max	Disc
1	1.92E-03	0.487	L2-L3
2	2.04E-03	0.518	L2-L3
3	1.85E-03	0.468	L1-L2
4	2.18E-03	0.550	L3-L4
5	2.19E-03	0.607	L3-L4

### Patient Models: COMSOL Methodology

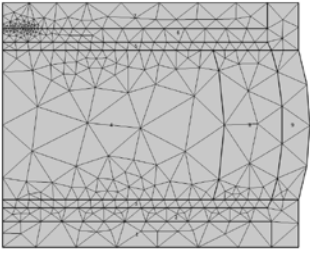
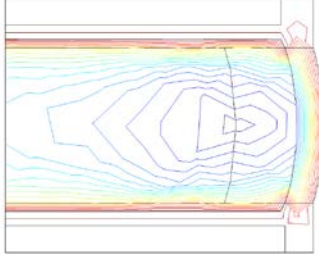
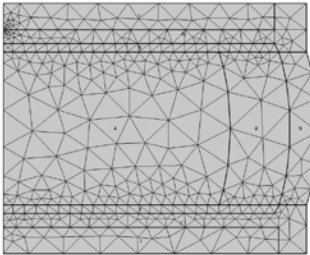
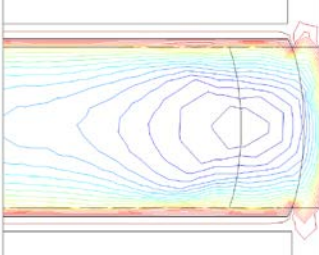
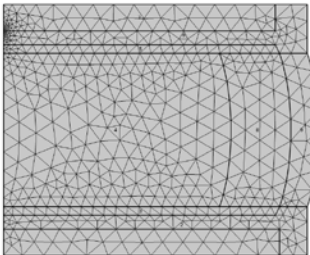
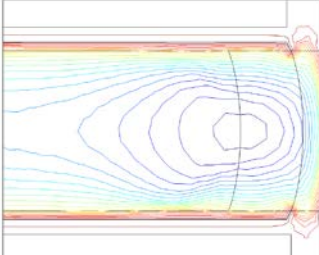
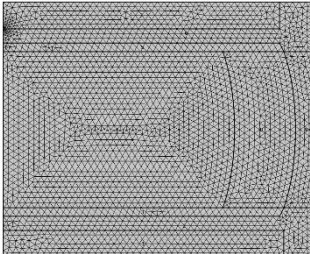
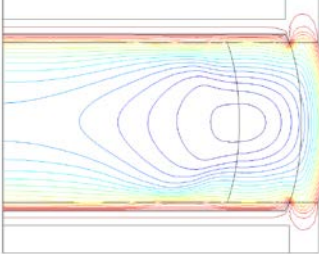
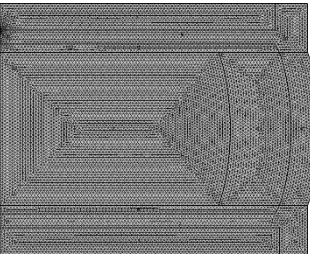
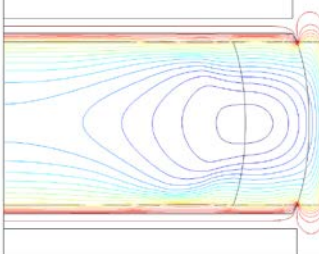
#### Model Geometry and Definitions

The transport model was developed using COMSOL Multiphysics (version 5.3a). COMSOL offers a variety of mesh types to accommodate a wide range of geometries: four tetrahedra (tets), hexahedra (bricks), triangular prisms (prisms), and pyramids. Within these types, there are also nine preset element size settings, ranging from “extremely fine” to “extremely coarse.” Sensitivity analysis results for mesh sizing are showcased in Figure 2. The chosen mesh density for this model was “extra fine.” Based on the results in Figure 2, it is apparent that finer meshes provide a negligible difference in the solution, in fact,



the mesh could have produced acceptable results up to two levels coarser.

**Figure 2** – COMSOL mesh sensitivity analysis with selected mesh sizes from extremely coarse to extremely fine.

Mesh Sizing	Solution Time	Mesh	Glucose Model Contour Result
“Extremely Coarse” Max: 0.00747 Min: 0.00113	9 s		
“Coarser” Max: 0.00294 Min: 1.36E-4	9 s		
“Normal” Max: 0.00152 Min: 6.79E-6	10 s		
“Extra Fine” Max: 4.53E-4 Min: 1.7E-6	14 s		
“Extremely Fine” Max: 2.26E-4 Min: 4.53E-7	23 s		



This level of accuracy was made possible by assuming axial symmetry and wrapping the 2D radial slice around the vertical axis to bring it into three dimensions. This is because, as the model complexity increases, coarser meshes are typically required to avoid excessive convergence times. It is also possible to spatially customize mesh density to reduce convergence times, while maintaining the desired level of accuracy in the region of interest. Later versions of this model will likely also require sacrifices in mesh density to reach convergence.

The metabolites of interest were identified as oxygen, glucose, and lactic acid. The primary mechanism for IVD cells to gain energy is through glycolysis. During glycolysis, glucose molecules are chemically cleaved into two lactate molecules. This metabolic process can lead to a buildup of lactate (lactic acid) inside the tissue, causing a drop in pH. This relationship between metabolism and pH is used to couple the concentration models of metabolites in the disc.<sup>17</sup>

The primary equations are based off of Fick's Law for diffusion and the general transport equation:

$$\frac{\partial C_A}{\partial t} = D_{AB} \left[ \frac{1}{r} \frac{\partial}{\partial r} \left( r \frac{\partial C_A}{\partial r} \right) + \frac{1}{r^2} \frac{\partial^2 C_A}{\partial \theta^2} + \frac{\partial^2 C_A}{\partial z^2} \right] + \dot{R}_A^v \quad (2)$$

Where R is in  $\left[\frac{\text{mol}}{\text{m}^3}\right]$  per hour (positive for production, and negative for consumption); C is the solute concentration (% for oxygen and  $\left[\frac{\text{mol}}{\text{m}^3}\right]$  for glucose and lactate); and D is the diffusion coefficient for the solute in the given solvent. Values for oxygen were originally given in kPa and converted to concentration using Henry's law. The maximum value for dissolved  $O_2$  was determined to be  $5.30 * 10^{-2} \left[\frac{\text{mol}}{\text{s}}\right]$  based on literature values for blood oxygen concentration.<sup>18</sup> This value was used to scale oxygen concentration in model equations such that oxygen was reported in units of % saturation.

For lactate generation:

$$\log(\text{Lactate Generation}) = -2.47 + 0.93 * pH + 0.16 * O_2 - 0.0058 * O_2^2 \quad (3)$$

Or:

$$\text{Lactate Generation} = e^{-2.47 + 0.93 * pH + 0.16 * O_2 - 0.0058 * O_2^2} \quad (4)$$

For oxygen consumption:

$$\text{Oxygen Consumption} = \frac{7.28 * O_2 * (pH - 4.95)}{1.46 + O_2 + 4.03 * (pH - 4.95)} \quad (5)$$

For glucose consumption, at any given point the consumption rate of glucose will be half that of the production rate of lactic acid (via the mechanism of glycolysis):

$$\text{Glucose Consumption} = \frac{1}{2} \text{Lactate Generation} \quad (6)$$

The distinct tissue types in and around disc each have specific production/consumption rates for each solute, scaled according to the cell density and water volume fraction of the given tissue (Table 2). The equations outlined above were also developed specifically for the NP. To apply them in the remaining areas of the disc, the equations were necessarily scaled using the ratio between the number of cells in the tissue and the number of cells in the NP. This ratio was included in the constants for scaling and unit conversion which were calculated for each tissue region in the model.

**Table 2** – Summary of cell density and water volume for each tissue region, including the

Region of Interest	Cell Density $\left[\frac{\text{million cells}}{\text{mm}^3}\right]$	Water Volume Fraction % ( $\epsilon$ )	Constant for Unit Conversion	Variable Assignment (COMSOL)
CEP	0.004	60	1.56E-05	C_CEP
NP	0.012	80	1.11E-06	C_NP
IA	0.006	73	2.50E-06	C_IA
OA	0.015	66	1.00E-05	C_OA

final unit conversion constants which combines appropriate ratios of cell density, and conversions from  $nmol$  to  $mol$ ,  $mm^3$  to  $m^3$  and  $h$  to  $s$ . Water volume fractions were used when converting oxygen concentration equations from units of kPa to %. IA and OA represent the inner and outer regions of the annulus fibrosis.

### Model Geometry and Boundary Conditions

In addition to the behavior of solutes in the bulk tissue, the model also accounts for the behavior of solutes at tissue boundaries. Three distinct boundaries were identified (Figure 2): the interface between the BEP and CEP ( $BC_1$ ), the interface between external tissues of the lumbar region and the OA ( $BC_2$ ), and the additional non-interface (no contact assumed) between the edges of the OA and the BEP ( $BC_3$ ). Boundary group 3 was assumed to be no-flux to correct for structural simplifications made when defining the disc

geometry. For all other boundaries a fraction of the external concentration was assumed to cross the boundary based on the relative conductivity in the tissue (Table 3).<sup>21</sup>

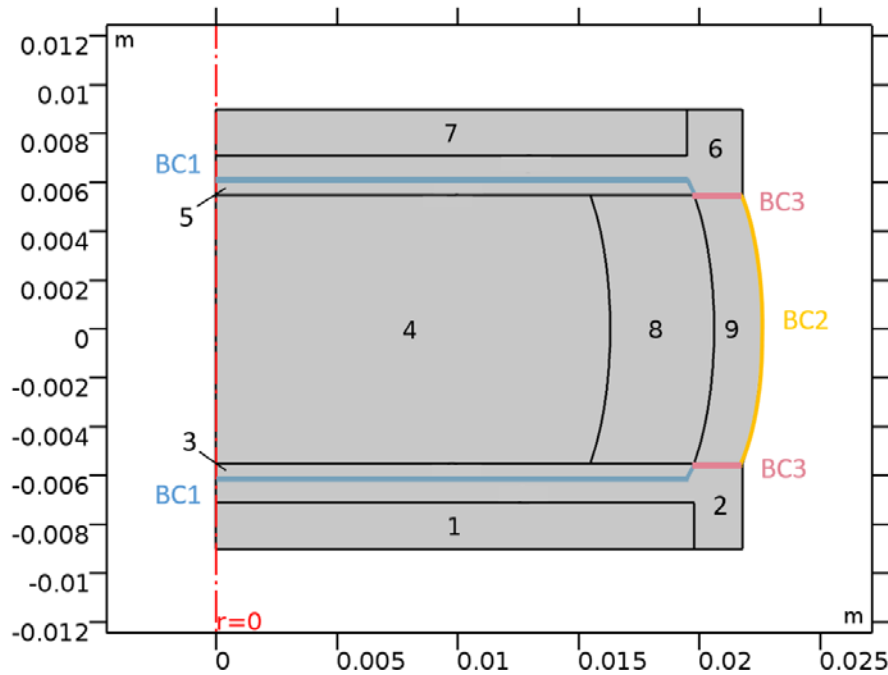


**Figure 2** – Disc geometry model including regions segmented for cancellous bone (1 & 7), cortical bone (2 & 6), the CEP (3 & 5), OA and IA (9 & 8), and the NP symmetry ( $r=0$ ) for the 2D axisymmetric model is shown in red. The 2D model will be wrapped around the y-axis, yielding a short cylinder (shown in Figure). Lengths are given in meters [m].

Furthermore, though the model is designed to incorporate patient data, this functionality is limited specifically to the NP region, all other regions (including the CEP, IA and OA) rely on previously determined values for diffusion (Table 3).<sup>18</sup> Due to a lack of data available for diffusion through cortical and cancellous bone, it was assumed that diffusion in the denser cortical bone is an order of magnitude lower than the cartilaginous endplate, while in the spongy cancellous bone, diffusion is an order of magnitude higher. This is a limitation of the current model that could be addressed in future work. Proper characterization of these properties is important due to the influence of the BEP on disc degeneration. As the disc degrades, one would likely see comparable changes to transport in the BEP as in the IVD. In fact, extreme changes in BEP diffusion properties could potentially be seen as a precursor to IVD degeneration. Further characterization in this area is necessary to achieve model validation.

**Table 3** – Diffusion coefficients (D) and boundary conditions (BC) for nutrients and metabolites in various regions of the disc as defined in Soukane et al, 2007.<sup>18</sup>  $BC_1 = 0.8 C_0$  for oxygen and lactate,  $BC_1 = 0.71 C_0$  for glucose, and  $BC_2 = 0.9 C_0$ , where  $C_{0, \text{Oxygen}} = 6.4 \text{ kPa}$ ,  $C_{0, \text{Glucose}} = 5.6 \text{ nmol/mm}^3$ , and  $C_{0, \text{Lactate}} = 1.0 \text{ nmol/mm}^3$ . Boundary 3 was assigned no-flux, as the two structures do not interact this way in the human body, this arrangement was merely a simplification for modeling purposes.

Region of Interest	Oxygen		Lactic Acid		Glucose	
	D [ $\frac{m^2}{s}$ ]	BC [kPa]	D [ $\frac{m^2}{s}$ ]	BC [ $\frac{mol}{m^3}$ ]	D [ $\frac{m^2}{s}$ ]	BC [ $\frac{mol}{m^3}$ ]
CEP	7.806E-10	5.1	3.139E-10	0.8	2.111E-10	4
IA	1.156E-09	-	4.667E-10	-	3.139E-10	-
OA	9.444E-10	5.8	3.806E-10	0.9	2.556E-10	5

For the patient-defined NP region, the data provides a value for water diffusion [ $\frac{m^2}{s}$ ] in the tissue. A method for calculating hindered solute diffusion in solvent-filled pores has been established by Renkin:<sup>29</sup>

$$\frac{D_{Ae}}{D_{AB}^0} = F_1(\varphi)F_2(\varphi)$$

This equation describes the diffusion of a solute molecule (species A) through a tiny capillary pore filled with a liquid solvent (species B). As size of the molecule increases, the diffusive transport of the solute through the solvent is hindered by the presence of the pore, specifically the pore wall. This hindrance is modeled with two correction factors,  $F_1$  and  $F_2$ , which are both functions of the reduced pore diameter ( $\varphi$ ), and are theoretically bounded by 0 and 1:

$$\varphi = \frac{d_s}{d_{\text{pore}}} = \frac{\text{solute molecular diameter}}{\text{pore diameter}}$$

The correction factor  $F_1(\varphi)$  is known as the steric partition coefficient and is based on geometric arguments for steric exclusion:

$$F_1(\varphi) = \frac{\text{flux area available to solute}}{\text{total flux area}} = \frac{\pi(d_{\text{pore}} - d_s)^2}{\pi d_{\text{pore}}^2} = (1 - \varphi)^2$$

The correction factor  $F_2(\varphi)$  is known as the hydrodynamic hindrance factor. It is based on a number of hydrodynamic calculations, including the hindered Brownian motion of the

solute within the solvent-filled pore. Renkin developed the following relationship for  $F_2(\varphi)$ , assuming the solute is a rigid sphere diffusing through a straight cylindrical pore:

$$F_2(\varphi) = 1 - 2.104\varphi + 2.09\varphi^3 - 0.95\varphi^5$$

Based on this, the ADC value for a given solute was scaled based on a ratio of literature values for diffusion of the solute in water, and the diffusion of water in water:

$$D_{W/T} \left[ \frac{m^2}{s} \right] * (D_{S/W} \left[ \frac{m^2}{s} \right] / D_{W/W} \left[ \frac{m^2}{s} \right]) = D_{W/T} \left[ \frac{m^2}{s} \right] * D_{S/W} \left[ \frac{m^2}{s} \right] = D_{S/T} \left[ \frac{m^2}{s} \right]$$

This relationship was determined based on the assumption that all four solutes (O<sub>2</sub>, glucose, lactate and water) were sufficiently small (on the scale of 100-1000 pm) relative to the pore to approximate  $F_1(\varphi)$  and  $F_2(\varphi)$  as the same across the solutes. This assumption allows for the following simplification:

$$D_{S/T} = D_{W/T} * \left( \frac{D_{S/W}}{D_{W/W}} \right) = D_{W/W} * F_1(\varphi) * F_2(\varphi) * \left( \frac{D_{S/W}}{D_{W/W}} \right) = D_{S/W} * F_1(\varphi) * F_2(\varphi)$$

Assuming the tissue is hydrated allow the diffusion of water in the tissue to be modeled as the hindered self-diffusion of water through a solvent filled pore, in which the constants  $F_1(\varphi)$  and  $F_2(\varphi)$  are already accounted for in the ADC. Accounting for the relative molecule size would require characterization of the specific tissue pore sizes, which is beyond the scope of this project. Using this method, scaling constants were generated for each solute (Table 4), such that the value determined for the diffusion of water in the patient's tissue could be converted to a value for the diffusion of glucose, lactate or oxygen in the tissue. See Appendix 3 for a summary of the constants and equations as they were inserted into COMSOL, including specific formatting and variable assignments.

**Table 4** – ADC conversion from water in tissue to nutrient/metabolite in tissue:

Solute	$D \left[ \frac{m^2}{s} \right]$
$D_{W/W}$	3.05E-9 <sup>30</sup>
$D_{G/W}$	9.17E-10 <sup>16</sup>
$D_{L/W}$	1.39E-09 <sup>16</sup>
$D_{O/W}$	3.00E-09 <sup>16</sup>
$D_{G/W}$	0.30
$D_{L/W}$	0.46
$D_{O/W}$	0.98

Finally, initial values for concentration of solutes in each region of the disc were determined from literature and assigned accordingly (Table 5). The maximum values those present in the vertebral blood supply, and the minimum values defined at the center of the disc where diffusion limitations are typically the most pronounced.

**Table 5** – Initial conditions for concentration of metabolites in various areas of the disc and adjacent tissue.

	BLOOD	CORT. BONE	CANC. BONE	CEP	AF	NP	DISC CENTER
Lactate $\left[\frac{mol}{s}\right]$		1.00E+00			5.00E+00		1.00E+01
Glucose $\left[\frac{mol}{s}\right]$		5.56E+00			2.80E+00		0.00E+00
Oxygen [kPa]		6.40E+00			3.55E+00		7.00E-01
Oxygen $\left[\frac{mol}{s}\right]$		5.30E-02			5.80E-03		8.60E-03

## RESULTS AND DISCUSSION

### Model Analysis

With the methods described previously, the diffusion behavior within a lumbar disc (Pfirrmann grade 2 and 1) was modeled for 5 patients. Disc selections are shown in Figure 2d of Appendix 2. An example of a typical 3D rendered model is shown in Figure 3. This model was generated by wrapping the 2D models of solute diffusion (Figure 4) around the y-axis of symmetry.

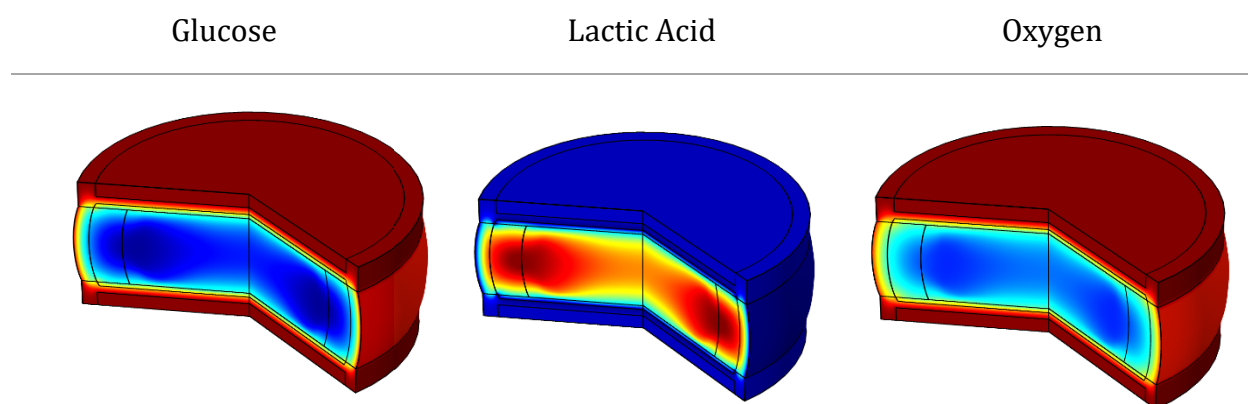


**Figure 3** – Characteristic 3D models for glucose, lactic acid and oxygen distribution within the disc for Patient #1. These were generated by wrapping the 2D models of nutrient/metabolite concentration shown in Figure 1-3 around the y-axis of symmetry. For individual concentration scales see Figure 4.

The models showcased in Figures 3 and 4 were run out to one week ( $t = 10,080$  min) and achieved what appeared to be steady state, with no discernable visual changes in the solute distribution within the disc towards the 50 hour mark. Thusly, the model represents the steady state distribution of nutrients and metabolites in the disc based on the patient's specific nutrient diffusivities. The glucose and oxygen models show a zone of low concentration which reaches a minimum at the interface between the IA and NP, meanwhile the lactic acid model show peak in the same area. This behavior agrees with that of previous investigations into general solute diffusion trends.<sup>18,31,32</sup> In these diffusion limited zones, a lack of sufficient diffusion leads to a critical deficit of nutrients, and a toxic buildup of metabolic products. The pH in these areas is at a minimum, and at beyond a certain point can begin to cause metabolic suppression and cell death.<sup>18,31</sup> For Glucose, IVD cell death has been shown to initiate at glucose levels below 0.5 mM, and at 0.2 mM all cells die in 3 days.<sup>22</sup> Cell death is also significant when pH drops to at or below 6.2.<sup>33</sup>



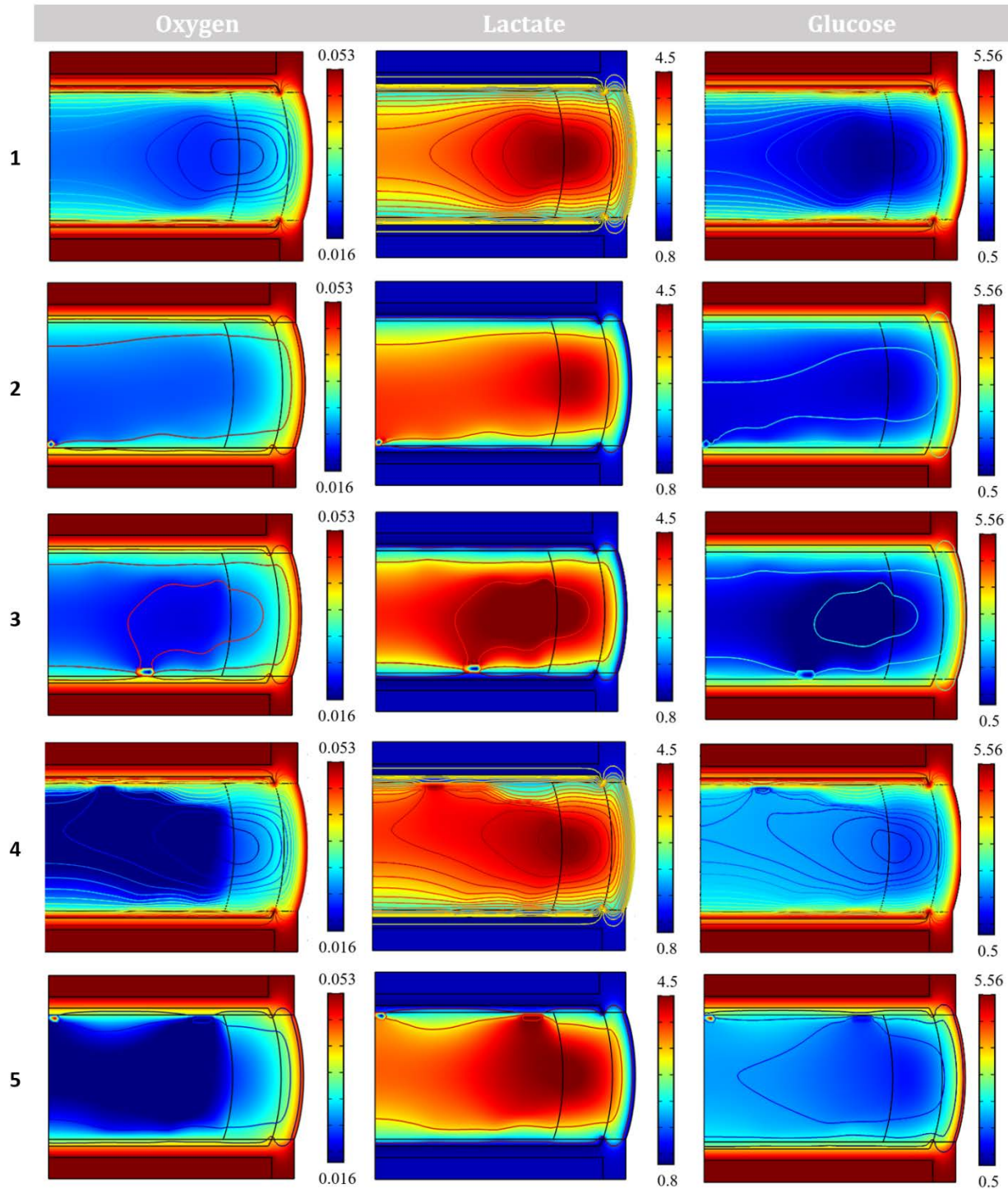


**Figure 4** – Characteristic distribution of oxygen (left), lactate (middle) and glucose (right) within the disc for patients 1-5. For oxygen, the scale ranges from a minimum of 0.016  $\left[\frac{mol}{m^3}\right]$  (deep blue) to a maximum of 0.053  $\left[\frac{mol}{m^3}\right]$  (deep red). For lactate, the scale ranges from a minimum of 0.8  $\left[\frac{mol}{m^3}\right]$  (deep blue) to a maximum of 4.5  $\left[\frac{mol}{m^3}\right]$  (deep red). For glucose, the scale ranges from a minimum of 0.5  $\left[\frac{mol}{m^3}\right]$  (deep blue) to a maximum of 5.56  $\left[\frac{mol}{m^3}\right]$  (deep red).



Though these general trends are consistent across all 5 patients - indicating consistent model performance - the specific trends of each patient are unique, which indicates successful integration of patient data. When comparing the specific trends for each solute across all 5 patients, distinct patterns are discernable, indicating that the individual morphology and physiological conditions of each patient's discs make an important difference to the metabolite gradients, even among discs of the same Pfirrmann grade.

### Model Limitations & Future Work

These results indicate both the legitimacy and importance of incorporating patient-specific parameters, however they also showcase key limitations of this particular modeling scheme. Visible in Figure 3 are computational “nodes” which indicate failure of the model to accommodate certain areas of data, or an issue of compatibility of the cropped image with the model geometry. This was determined to be a likely product of pixel limitations (poor resolution) of the DWI image. Future work should focus on collecting higher resolution images to facilitate better compatibility between model geometries and diffusion maps. Note that this study used images from a 1.5 T MRI, leaving much room for improvement in this area. Additionally, the model assumes a fixed cell density in each region based on values identified in previous work for cell concentration in various disc tissues. The solution therefore does not account for how cell death due to “dead zones” of nutrients would affect the nutrient distribution within the disc. Future work could investigate model sensitivity to cell density, or attempt to model the dynamic changes in cell density associated with patient specific nutrient gradients and degradation.

Furthermore, this model is only valid for patients with discs Pfirrmann grade 2 or below. This is because, at higher levels of degradation, relatively extreme morphological changes can start manifesting, causing incompatibility with the developed COMSOL geometry, which was modeled off of the dimensions of a healthy disc. To address this issue is essential because typically back pain is associated with the more extreme degradation (Pfirrmann grade 3+). Future work should focus on generating a geometry directly from the patient's morphology as captured by the MRI. This would eliminate the need to define a separate, generic disc geometry in COMSOL, and would lend more accuracy and applicability to the model as a whole. Additionally, this model only incorporates patient data into the region of the NP. This is because this region is the one best captured by DWI. However, incorporating

data from the other regions of the disc (IA and OA) could prove extremely valuable, particularly in the case of disc rupture, or endplate calcification. Future work should explore methods of collecting diffusivity data from other regions of the disc. This process could be part of a larger effort to validate model predictions through disc tissue biopsy and analysis in animal models. This analysis could include glucose, oxygen and lactate/pH concentration measurements in specific areas of the disc, followed by direct comparison with the concentration distributions predicted by the model.

Finally, a quantified comparison of ADC and model results is desired to better evaluate the utility of the model developed here. Future work should seek a quantitative measure of patient-to-patient variability for both the ADC and the model solution. One possible method could be to evaluate the steady state model nutrient distributions with the same method used to evaluate the DWI image, i.e. find the minimum and maximum value, average value, and standard deviation of the results and compare that to the ADC. Comparing these values should allow the novelty/utility of the model to be quantified based on the difference from the raw ADC data.

## CONCLUSION

This work describes a method for incorporating patient data into a nutrient transport model of the intervertebral disc. Results show distinct diffusion behavior between patients, even within discs of the same Pfirrmann grade. The importance of the distinct disc morphologies and physiological environments of each patient to the diffusion gradients in the disc is readily apparent. Patient-specific models could allow clinicians to further personalize treatments to the patient. Pending further development, this model could allow clinicians to account for the impact of increasing cell activity or density in a nutrient-starved environment, namely, the generation of dead zones. Clinicians could use this tool to look for critical concentrations and pH's in the patient's discs (i.e. levels below which cells cannot survive). If levels are already low enough to indicate cell death, these patients would not be candidates for cell injection-based therapies. For patients without a dead zone - who are therefore candidates for cell therapy - the model can be used to determine proper dosing via iteratively increasing cell concentration until the patient develops a dead zone. This functionality indicates that patient-specific models could prove valuable in a clinical setting when predicting patient outcomes or treatment options.

## BIBLIOGRAPHY

1. Freburger JK, Holmes GM, Agans RP, et al. The Rising Prevalence of Chronic Low Back Pain. *Arch Intern Med*. 2009;169(3):251-258. doi:10.1001/archinternmed.2008.543
2. Hoy D, March L, Brooks P, et al. The global burden of low back pain: estimates from the Global Burden of Disease 2010 study. *Ann Rheum Dis*. 2014;73(6):968-974. doi:10.1136/annrheumdis-2013-204428
3. Crow WT, Willis DR. Estimating Cost of Care for Patients With Acute Low Back Pain: A Retrospective Review of Patient Records. *J Am Osteopath Assoc*. 2009;109(4):229-233. doi:10.7556/jaoa.2009.109.4.229
4. Huang Y-C, Urban JPG, Luk KDK. Intervertebral disc regeneration: do nutrients lead the way? *Nat Rev Rheumatol*. 2014;10(9):561+.
5. Alkhatib B, Rosenzweig DH, Krock E, et al. Acute mechanical injury of the human intervertebral disc: link to degeneration and pain. *Eur Cell Mater*. 2014;28:98-110.
6. Hughes SPF, Freemont AJ, Hukins DWL, McGregor AH, Roberts S. The pathogenesis of degeneration of the intervertebral disc and emerging therapies in the management of back pain. *J Bone Joint Surg Br*. 2012;94-B(10):1298-1304. doi:10.1302/0301-620X.94B10.28986
7. Urban JP, Roberts S. Degeneration of the intervertebral disc. *Arthritis Res Ther*. 2003;5(3):120-130. doi:10.1186/ar629
8. Urrutia J, Besa P, Campos M, et al. The Pfirrmann classification of lumbar intervertebral disc degeneration: an independent inter- and intra-observer agreement assessment. *Eur Spine J Off Publ Eur Spine Soc Eur Spinal Deform Soc Eur Sect Cerv Spine Res Soc*. 2016;25(9):2728-2733. doi:10.1007/s00586-016-4438-z
9. Pfirrmann CW, Metzdorf A, Zanetti M, Hodler J, Boos N. Magnetic resonance classification of lumbar intervertebral disc degeneration. *Spine*. 2001;26(17):1873-1878.
10. Shapiro IM, Risbud MV. *The Intervertebral Disc: Molecular and Structural Studies of the Disc in Health and Disease*. Springer; 2013. <https://books.google.com/books?id=SFEbswEACAAJ>.
11. Biochemistry of the intervertebral disc. - PubMed - NCBI. <https://www.ncbi.nlm.nih.gov/pubmed/8364983>. Accessed March 5, 2019.
12. Urban J PG, Smith S CT, Fairbank J CT. Nutrition of the Intervertebral Disc. *Spine*. 2004;29(23):2700–2709.
13. Urban JPG, Grunhagen T, Wilde G, Soukane DM, Shirazi-Adl SA, Urban JPG. Nutrient supply and intervertebral disc metabolism. *J Bone Jt Surg*. 2006;88(Supplement 2):30. doi:10.2106/JBJS.E.01290
14. Kolluru GK, Bir SC, Kevil CG. Endothelial Dysfunction and Diabetes: Effects on Angiogenesis, Vascular Remodeling, and Wound Healing. *Int J Vasc Med*. 2012;2012. doi:10.1155/2012/918267
15. Cardiovascular Diseases - How Tobacco Smoke Causes Disease: The Biology and Behavioral Basis for Smoking-Attributable Disease - NCBI Bookshelf. <https://www.ncbi.nlm.nih.gov/books/NBK53012/>. Accessed March 18, 2019.

16. Magnier C, Boiron O, Wendling-Mansuy S, Chabrand P, Deplano V. Nutrient distribution and metabolism in the intervertebral disc in the unloaded state: A parametric study. *J Biomech.* 2009;42(2):100-108. doi:10.1016/j.jbiomech.2008.10.034
17. Bibby S RS, Jones D A, Ripley R M, Urban J PG. Metabolism of the Intervertebral Disc: Effects of Low Levels of Oxygen, Glucose, and pH on Rates of Energy Metabolism of Bovine Nucleus Pulposus Cells. *Spine.* 2005;30(5):487–496.
18. Mokhbi Soukane D, Shirazi-Adl A, Urban JPG. Computation of coupled diffusion of oxygen, glucose and lactic acid in an intervertebral disc. *J Biomech.* 2007;40(12):2645–2654.
19. Ferguson SJ, Ito K, Nolte L-P. Fluid flow and convective transport of solutes within the intervertebral disc. *J Biomech.* 2004;37(2):213–221. doi:10.1016/S0021-9290(03)00250-1
20. Malandrino A, Noailly J, Lacroix D. The Effect of Sustained Compression on Oxygen Metabolic Transport in the Intervertebral Disc Decreases with Degenerative Changes (Sustained Compression on Oxygen Transport in IVD). *PLoS Comput Biol.* 2011;7(8):e1002112. doi:10.1371/journal.pcbi.1002112
21. Jackson AR, Yuan T-Y, Huang C-Y, Gu WY. A Conductivity Approach to Measuring Fixed Charge Density in Intervertebral Disc Tissue. *Ann Biomed Eng.* 2009;37(12):2566-2573. doi:10.1007/s10439-009-9792-0
22. Zhu Q, Jackson AR, Gu WY. Cell viability in intervertebral disc under various nutritional and dynamic loading conditions: 3d Finite element analysis. *J Biomech.* 2012;45(16):2769-2777. doi:https://doi.org/10.1016/j.jbiomech.2012.08.044
23. Gullbrand E, Peterson T, Ahlborn P, et al. ISSLS Prize Winner: Dynamic Loading–Induced Convective Transport Enhances Intervertebral Disc Nutrition. *Spine.* 2015;40(15):1158–1164. doi:10.1097/BRS.0000000000001012
24. Munter B. Demonstration of the Effects of Traction Therapy on the Nutrient Supply of the Lumbar Intervertebral Disc: A Mathematical Model. 2016.
25. Failed back surgery syndrome: current perspectives. - PubMed - NCBI. <https://www.ncbi.nlm.nih.gov/pubmed/27853391>. Accessed March 19, 2019.
26. Belykh E, Kalinin AA, Patel AA, et al. Apparent diffusion coefficient maps in the assessment of surgical patients with lumbar spine degeneration. *PLOS ONE.* 2017;12(8):e0183697. doi:10.1371/journal.pone.0183697
27. Chilla GS, Tan CH, Xu C, Poh CL. Diffusion weighted magnetic resonance imaging and its recent trend—a survey. *Quant Imaging Med Surg.* 2015;5(3):407-422. doi:10.3978/j.issn.2223-4292.2015.03.01
28. Le Bihan D, Breton E. In vivo magnetic resonance imaging of diffusion. *Comptes Rendus Seances Acad Sci Ser 2.* 1985;301(15):1109-1112.
29. Fundamentals of Momentum, Heat, and Mass Transfer, Revised 6th Edition. Wiley.com. <https://www.wiley.com/en-us/Fundamentals+of+Momentum%2C+Heat%2C+and+Mass+Transfer%2C+Revised+6th+Edition-p-9781118947463>. Accessed March 19, 2019.

30. Harris KR, Woolf LA. Pressure and temperature dependence of the self diffusion coefficient of water and oxygen-18 water. *J Chem Soc Faraday Trans 1 Phys Chem Condens Phases*. 1980;76(0):377-385. doi:10.1039/F19807600377
31. Das DB, Welling A, Urban JPG, Boubriak OA. Solute Transport in Intervertebral Disc. *Ann N Y Acad Sci*. 2009;11611(1):44–61.
32. Soukane DM, Shirazi-Adl A, Urban JP. Analysis of Nonlinear Coupled Diffusion of Oxygen and Lactic Acid in Intervertebral Discs. *J Biomech Eng*. 2005;127(7):1121-1126. doi:10.1115/1.2073674
33. Gilbert HTJ, Hodson N, Baird P, Richardson SM, Hoyland JA. Acidic pH promotes intervertebral disc degeneration: Acid-sensing ion channel -3 as a potential therapeutic target. *Sci Rep*. 2016;6. doi:10.1038/srep37360

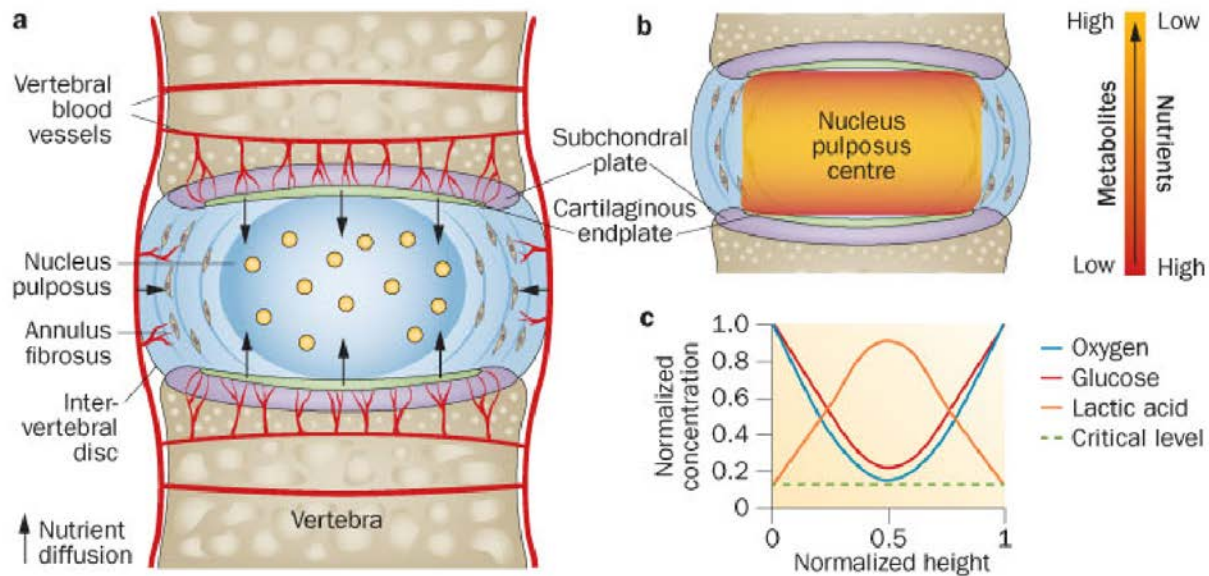
## APPENDICES

### Appendix 1 – Index of Abbreviations

ABBREVIATION	TERM
<b>IVD</b>	Intervertebral disc
<b>MRI</b>	Magnetic resonance imaging
<b>DWI</b>	Diffusion weighted imaging
<b>ADC</b>	Apparent diffusion coefficient
<b>LBP</b>	Lower back pain
<b>AF</b>	Annulus Fibrosis
<b>OA</b>	Outer annulus
<b>IA</b>	Inner annulus
<b>NP</b>	Nucleus pulposus
<b>CEP</b>	Cartilaginous endplate
<b>BEP</b>	Bony endplate
<b>ECM</b>	Extracellular matrix

## Appendix 2 – Supplemental Figures

**Figure 2a:** From Huang et al (2014): Pathways of nutrient supply in a normal intervertebral disc.<sup>4</sup>



- a. From Huang et al (2014): "Cells of the avascular disc nucleus pulposus and inner annulus fibrosis are supplied by vertebral blood vessels. Capillaries penetrate the subchondral plate through marrow spaces and terminate in loops at the junction of the subchondral plate and cartilaginous endplate. Nutrients (e.g. oxygen and glucose) diffuse from the capillary bed through the cartilaginous endplate under gradients arising from metabolic demands of disc cells, while metabolic wastes (e.g. lactic acid) diffuse in the reverse direction. Cells of the outer annulus fibrosis are supplied by capillaries from blood vessels in the surrounding soft tissues that penetrate a few millimeters into the disc."<sup>4</sup>
- b. From Huang et al (2014): "The center of the disc has the lowest levels of nutrients and highest concentration of metabolites."<sup>4</sup>
- c. From Huang et al (2014): "Schematic showing normalized concentration gradients of glucose, oxygen, and lactic acid across the nucleus, endplate to endplate. Nutrient concentrations must remain above the critical levels to maintain cell viability and activity."<sup>4</sup>

**Figure 2b:** Sectioned and labeled porcine lumbar IVD. Disc was provided by Dr. Morgan Giers (Oregon State University). and isolation and sagittal slicing performed by undergraduate research assistance Rees Rosene. Color coded section geometry provided for reference: cancellous bone (purple), cortical bone (red), the CEP (blue), OA and IA (orange and yellow), and the NP (green). The axis of symmetry ( $r=0$ ) for the 2D axisymmetric model is shown in red.

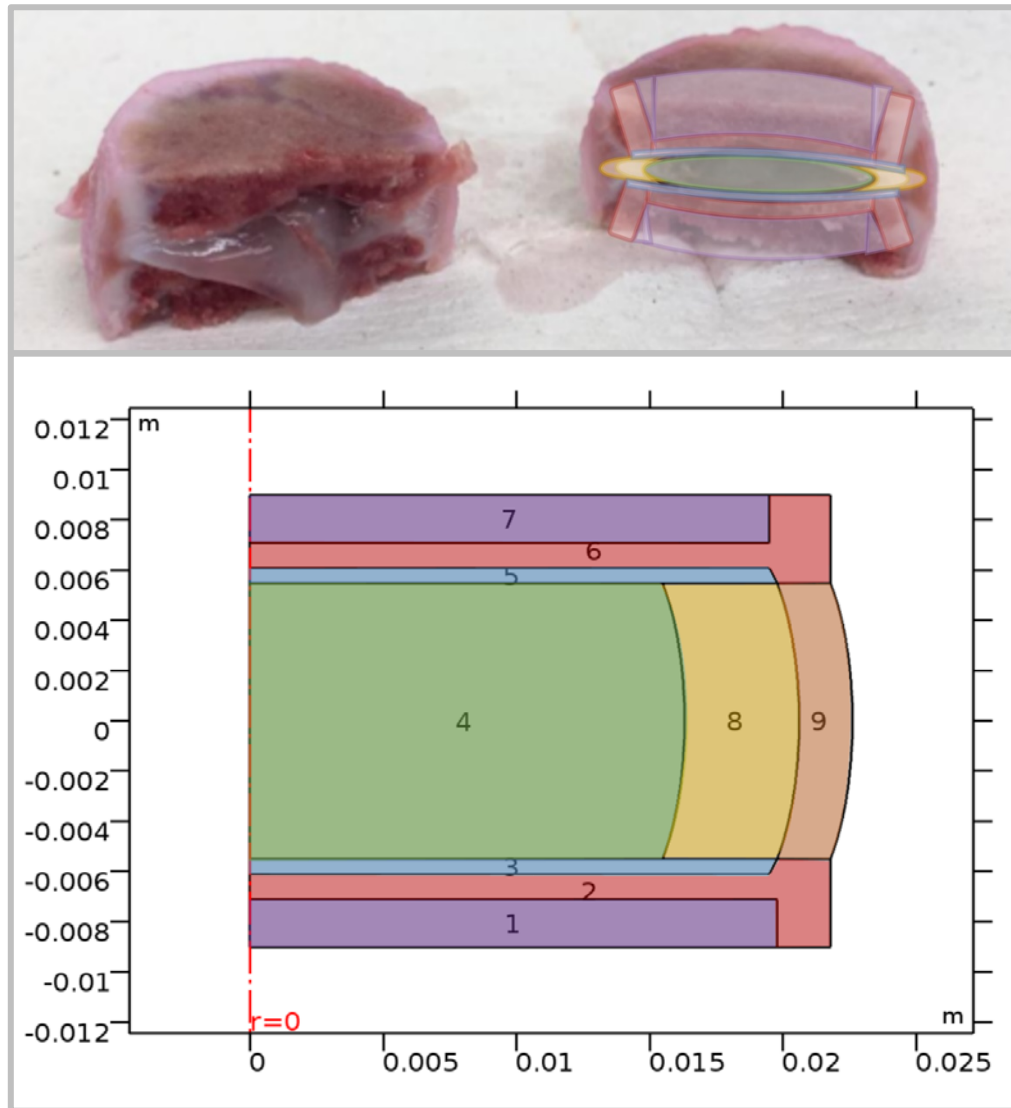




**Figure 2c:** T2 images for patients 1-5. Discs selected for modeling are highlighted in red.

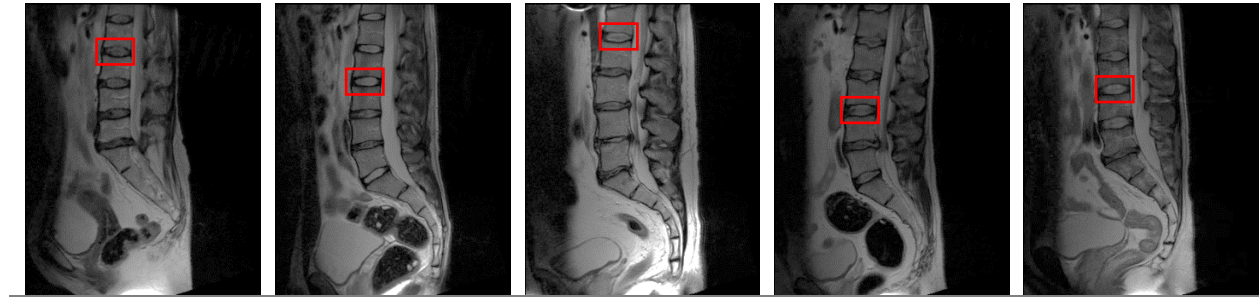
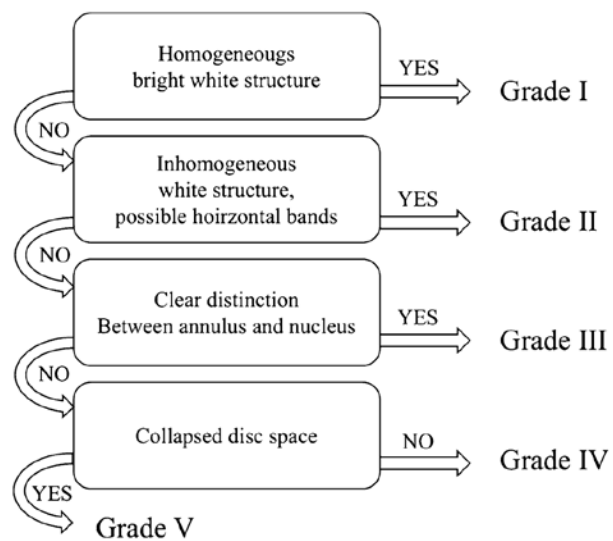


**Figure 2d:** From Urrutia et al: Sn algorithm used for grading lumbar disc degeneration<sup>8</sup>



### Appendix 3 – COMSOL Constants and Equations

**Table 3a** – Summary of variables used in model, including their value, unit, and a short description.

COMSOL Variables	Value	Unit	Description
ADCMAP	an1(r,z)		References the ADC image in cylindrical geometry
C_CEP	1.56E-05		Ratio of cell density (CEP/NP) * conversion from nmol to mol * conversion from mm <sup>3</sup> to m <sup>3</sup> * conversion from h to s <sup>32</sup>
C_IAF	2.50E-06		Ratio of cell density (AF/NP) * conversion from nmol to mol * conversion from mm <sup>3</sup> to m <sup>3</sup> * conversion from h to s <sup>32</sup>
C_NP	1.11E-06		Ratio of cell density (NP/NP) * conversion from nmol to mol * conversion from mm <sup>3</sup> to m <sup>3</sup> * conversion from h to s <sup>32</sup>
C_OAF	1.00E-05		Ratio of cell density (AF/NP) * conversion from nmol to mol * conversion from mm <sup>3</sup> to m <sup>3</sup> * conversion from h to s <sup>32</sup>
CD_CEP	1.50E-02	million cells/mm <sup>3</sup>	Cell Density <sup>32</sup>
CD_IA	0.006	million cells/mm <sup>3</sup>	Cell Density <sup>32</sup>
CD_NP	0.004	million cells/mm <sup>3</sup>	Cell Density <sup>32</sup>
CD_OA	0.012	million cells/mm <sup>3</sup>	Cell Density <sup>32</sup>
DG_AF	2.85E-10	m <sup>2</sup> /s	Diffusion constant for glucose <sup>32</sup>
DG_CEP	2.11E-10	m <sup>2</sup> /s	Diffusion constant for glucose <sup>32</sup>
DG_CNB	2.11E-09	m <sup>2</sup> /s	Diffusion constant for glucose <sup>32</sup>
DG_CTB	2.11E-11	m <sup>2</sup> /s	Diffusion constant for glucose <sup>32</sup>
DG_NP	ADCMAP		References image (Literature value = 1.81E-09 <sup>32</sup> )
DGW	0.98		Conversion factor for ADC data to glucose
DL_AF	4.24E-10	m <sup>2</sup> /s	Diffusion constant for lactate <sup>32</sup>
DL_CEP	3.14E-10	m <sup>2</sup> /s	Diffusion constant for lactate <sup>32</sup>
DL_CNB	3.14E-09	m <sup>2</sup> /s	Diffusion constant for lactate <sup>32</sup>
DL_CTB	3.14E-11	m <sup>2</sup> /s	Diffusion constant for lactate <sup>32</sup>
DL_NP	ADCMAP		References image (Literature value = 5.61E-10 <sup>32</sup> )
DLW	0.46		Conversion factor for ADC data to lactate
DO_AF	1.15E-09	m <sup>2</sup> /s	Diffusion constant for oxygen <sup>32</sup>
DO_CEP	5.08E-10	m <sup>2</sup> /s	Diffusion constant for oxygen <sup>32</sup>
DO_CNB	5.08E-09	m <sup>2</sup> /s	Diffusion constant for oxygen <sup>32</sup>
DO_CTB	5.08E-11	m <sup>2</sup> /s	Diffusion constant for oxygen <sup>32</sup>
DO_NP	ADCMAP		References image (Literature value = 1.65E-09 <sup>32</sup> )
DOW	0.98		Conversion factor for ADC data to oxygen
E_CEP	0.6		Water Content <sup>32</sup>
E_IA	0.73		Water Content <sup>32</sup>

<b>E_NP</b>	<b>0.8</b>		<b>Water Content<sup>32</sup></b>
<b>E_OA</b>	<b>0.66</b>		<b>Water Content<sup>32</sup></b>
<b>G</b>	<b>c_g</b>	<b>mol/m<sup>3</sup></b>	<b>Concentration of glucose</b>
<b>L</b>	<b>c_l</b>	<b>mol/m<sup>3</sup></b>	<b>Concentration of lactate</b>
<b>log</b>	<b>10</b>		<b>Exponent value for glucose reaction term</b>
<b>ltog</b>	<b>-0.0005</b>		<b>Conversion factor from L to G reaction</b>
<b>O</b>	<b>c_o</b>	<b>mol/m<sup>3</sup></b>	<b>Concentration of oxygen</b>
<b>O2_MAX</b>	<b>0.053</b>	<b>mol/m<sup>3</sup></b>	<b>Maximum O2 concentration in blood (6.4 kPa converted to a concentration using Henry's Law) <sup>32</sup></b>
<b>R_G</b>	<b>tdsg.R_c_g</b>	<b>mol/(m<sup>3</sup>·s)</b>	<b>References reaction term for glucose</b>

**Tables 3b-d – Reaction terms as they are used in the COMSOL model.**

**Table 3b**

<b>Region of Interest</b>	<b>Lactic Acid</b>
CEP	$(-1.5) \cdot (\text{tdsg.R\_c\_g})$
NP	$(-1.5) \cdot (\text{tdsg.R\_c\_g})$
IA	$(-1.5) \cdot (\text{tdsg.R\_c\_g})$
OA	$(-1.5) \cdot (\text{tdsg.R\_c\_g})$

**Table 3c**

<b>Region of Interest</b>	<b>Oxygen</b>
CEP	$\frac{-C\_CEP \cdot E\_CEP \cdot ((7.28 \cdot (O/O2\_MAX) \cdot ((8.05 - 0.1 \cdot (-L)) - 4.95)) / (1.46 + (O/O2\_MAX) + 4.03 \cdot ((7.4 - 0.1 \cdot (-L)) - 4.95)))}{}$
NP	$\frac{-C\_NP \cdot E\_NP \cdot ((7.28 \cdot (O/O2\_MAX) \cdot ((8.05 - 0.1 \cdot (L)) - 4.95)) / (1.46 + (O/O2\_MAX) + 4.03 \cdot ((8.05 - 0.1 \cdot (L)) - 4.95)))}{}$
IA	$\frac{-C\_IAF \cdot E\_IA \cdot ((7.28 \cdot (O/O2\_MAX) \cdot ((7.4 - 0.1 \cdot (L)) - 4.95)) / (1.46 + (O/O2\_MAX) + 4.03 \cdot ((7.4 - 0.1 \cdot (L)) - 4.95)))}{}$
OA	$\frac{-C\_OAF \cdot E\_OA \cdot ((7.28 \cdot (O/O2\_MAX) \cdot ((7.4 - 0.1 \cdot (L)) - 4.95)) / (1.46 + (O/O2\_MAX) + 4.03 \cdot ((7.4 - 0.1 \cdot (L)) - 4.95)))}{}$

Table 3d

Region of Interest	Glucose
CEP	$\text{ltog} * C_{\text{CEP}} * \log^{\wedge}((-2.47) + ((0.93) * (8.05 - 0.1 * L)) + ((0.16) * (O/O2\_MAX)) - ((0.0058) * ((O/O2\_MAX)^2)))$
NP	$\text{ltog} * C_{\text{NP}} * \log^{\wedge}((-2.47) + ((0.93) * (8.05 - 0.1 * L)) + ((0.16) * (O/O2\_MAX)) - ((0.0058) * ((O/O2\_MAX)^2)))$
IA	$\text{ltog} * C_{\text{IAF}} * \log^{\wedge}((-2.47) + ((0.93) * (8.05 - 0.1 * L)) + ((0.16) * (O/O2\_MAX)) - ((0.0058) * ((O/O2\_MAX)^2)))$
OA	$\text{ltog} * C_{\text{OAF}} * \log^{\wedge}((-2.47) + ((0.93) * (8.05 - 0.1 * L)) + ((0.16) * (O/O2\_MAX)) - ((0.0058) * ((O/O2\_MAX)^2)))$